Highlights

Probing Protein Adsorption onto Polymer-Stabilized Silver Nanocolloids towards a Better Understanding on the Evolution and Consequences of Biomolecular Coronas

- Polymer-coated AgNPs can be highly resistant to protein binding
- PVP and PEO-*b*-P2VP shells repel model protein adsorption
- PEI-coated AgNPs are susceptible to BSA adsorption
- BSA adsorption onto AgNPs@PEI is driven by van der Waals and hydrogen bonding
- Protein adsorption duly influences biomedical applications of AgNPs

Table of Contents Entry (TOC)

Probing Protein Adsorption onto Polymer-Stabilized Silver Nanocolloids towards a Better Understanding on the Evolution and Consequences of Biomolecular Coronas

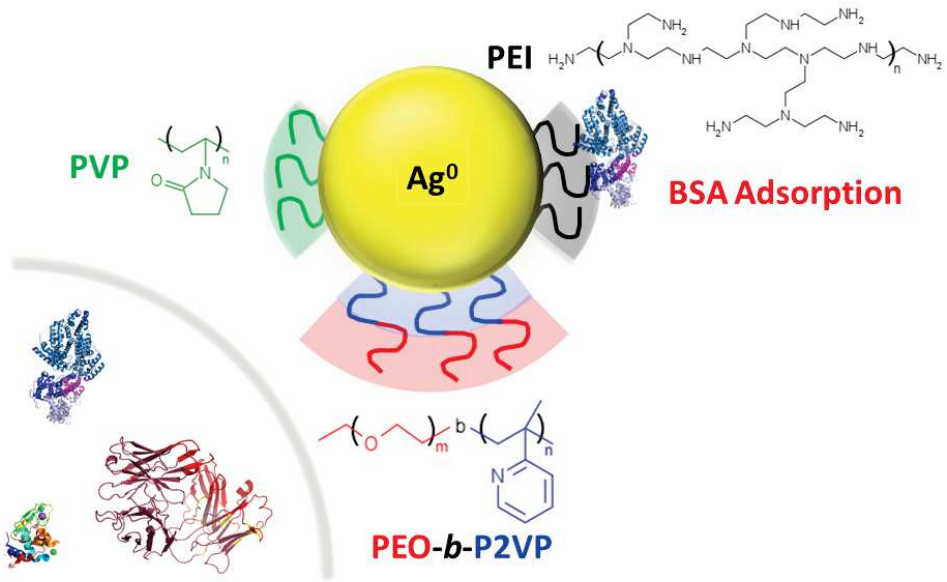

Probing Protein Adsorption onto Polymer-Stabilized Silver Nanocolloids towards a Better Understanding on the Evolution and Consequences of Biomolecular Coronas

Carin C. S. Batista, [a] *Lindomar J. C. Albuquerque,* [a] *Alessandro Jäger,* [b] *Petr Stepánek* [b] *and Fernando C. Giacomelli* [a,*]

[a] Centro de Ciências Naturais e Humanas, Universidade Federal do ABC, Santo André, Brazil.

[b] Institute of Macromolecular Chemistry, Czech Academy of Sciences, Prague, Czech Republic.

*Corresponding Author: Fernando Carlos Giacomelli

e-mail: fernando.giacomelli@ufabc.edu.br

ABSTRACT

The use of noble metal nanoparticles in biomedical and biotechnological applications is nowadays well established. Particularly, silver nanoparticles (AgNPs) were proven to be effective for instance as a biocide agent. They also find applications in tumor therapies and sensing applications being encouraging tools for *in-vivo* imaging. In this framework, whenever they are in contact with living systems, they are rapidly coated by a protein corona thereby influencing a variety of biological events including cellular uptake, blood circulation lifetime, cytotoxicity and, ultimately, the therapeutic effect. Taking these considerations into account, we have explored the behavior of polymer-coated AgNPs in model protein environments focusing on the self-development of protein coronas. The polymers polyethyleneimine (PEI), polyvinylpyrrolidone (PVP) and poly(2-vinyl pyridine)-*b*-poly(ethylene oxide) (PEO-*b*-P2VP) were used as stabilizing agents. The chemical nature of the polymer capping remarkably influences the behavior of the hybrid nanomaterials in protein environments. The PEO-*b*-P2VP and PVP-stabilized AgNPs are essentially inert to the model proteins adsorption. On the other hand, the PEI-stabilized AgNPs interact strongly with bovine serum albumin (BSA). Nevertheless, the same silver colloids were evidenced to be stable in IgG and lysozyme environments. The BSA adsorption into the PEI-stabilized AgNPs is most probably driven by hydrogen bonding and van der Waals interactions as suggested by isothermal titration calorimetry data. The development of protein coronas around the AgNPs may have relevant implications in a variety of biological events. Therefore, further investigations are currently underway to evaluate the influence of its presence on the cytotoxicity, hemolytic effects and biocide properties of the produced hybrid nanomaterials.

INTRODUCTION

The use of nanoparticle-based technologies is nowadays a well-established platform and it is being progressively inserted into the biomedical field with outstanding impacts in detection, diagnosis, imaging and therapy.[1–3] The potential use of noble metal nanoparticles (for instance, silver and gold colloids) has been investigated to the greatest extent particularly due to their facile chemical synthesis. The biocide property of AgNPs is nowadays well established [4–7] although the actual mechanism of action is still debated.[8–10] The AgNPs were also reported to be effective against a variety of viruses and they are also useful in tumor therapies demonstrating inhibition of cell proliferation and tumor progression.[3] Additionally, taking into account their light absorption at the surface plasmon resonance (SPR) wavelength, the optical properties of AgNPs enable their use in sensing applications and therefore, they are an encouraging tool for *in-vivo* imaging.[11,12] In this framework, whenever these nanomaterials are administrated intravenously, they may become rapidly coated by a protein corona [13–16] thereby influencing a variety of biological events including biodistribution, cellular uptake, blood circulation lifetime, cytotoxicity, targeting capability, mitochondrial energy metabolism, oxidative stress response and the therapeutic effect.[17–22] Accordingly, investigations regarding the interaction of AgNPs with biologically-relevant proteins is of due importance. Primarily, the use of capping agents that reduces protein fouling is more interesting to keep their biological activity during blood circulation.

The self-development of protein coronas around nanoparticles can be governed by different intermolecular forces including the contributions of London dispersion, Coulomb forces, van der Waals interactions, hydrogen bonding and hydrophobic

effects.[23,24] These intermolecular forces determine the formation, chemical nature, binding affinity and binding ratio of adsorbed proteins. The chemical nature and the structural characteristics of the biomolecular coronas are linked to the structural features of the nanomaterial (size, shape, chemical nature of the stabilizer, surface charge, surface curvature, etc.).[25–28] Therefore, in order to make steps further in this field, we have evaluated the interaction of polymer-capped AgNPs with model proteins. Taking into account that protein interaction depends on the surface chemistry of the nanomaterials, herein we investigated the protein adsorption at the surface of AgNPs stabilized by PEI (polyethylenimine), PVP (polyvinylpyrrolidone) and PEO-*b*-P2VP (poly(ethylene oxide) -*b*- poly(2-vinyl pyridine)). The particle coating by PVP and PEO-based polymers are usually alternatives for the passivation of surfaces whereas PEI is frequently considered towards the manufacturing of nano-sized silver colloids with antimicrobial activity because not only silver, but also PEI [29] is known to hold biocide properties. Therefore, synergic effects might be expected depending on the protocol of nanoparticle preparation.[30] Additionally, PEI can act efficiently and simultaneously as reductant and electrostatic stabilizer in the synthesis of hybrid inorganic-organic assemblies.[31] The behavior of the nano-sized silver colloids at bovine serum albumin (BSA), immunoglobulin G (IgG) and lysozyme environments was evaluated. These proteins were selected because they hold remarkably different sizes and isoelectric points. The investigations have been conducted by using scattering techniques, isothermal titration calorimetry (ITC), UV-Vis and fluorescence spectroscopy. The scattering techniques and UV-vis spectroscopy were employed to probe changes in size whereas by ITC it has been evaluated the thermodynamics related to protein adsorption. The fluorescence spectroscopy data was used to confirm protein adsorption and access the protein quenching mechanism. The reported results evidenced

that the capping agents influence remarkably the protein adsorption event and these findings are of due relevance for a better understanding on the evolution of biomolecular coronas around nanomaterials towards the rational design of nanoparticles for biomedical applications. The manufacturing of assemblies resistant to protein adsorption is supposed to help them preserve their biological activity while circulating in biological milieus and simultaneously avoid their aggregation and fast clearance.

EXPERIMENTAL

Chemicals

Silver nitrate ($AgNO_3$), sodium borohydride ($NaBH_4$), PEI (polyethyleneimine) and PVP (polyvinylpyrrolidone) were all purchased from Sigma-Aldrich whereas PEO-*b*-P2VP (poly(ethylene oxide)-*b*-poly(2-vinyl pyridine) was purchased from Polymer Source Inc. The water was previously pretreated with Milli-Q® Plus System (Millipore Corporation). The Figure 1 portrays the molecular structure of the stabilizing polymers and the Table 1 their molecular characteristics.

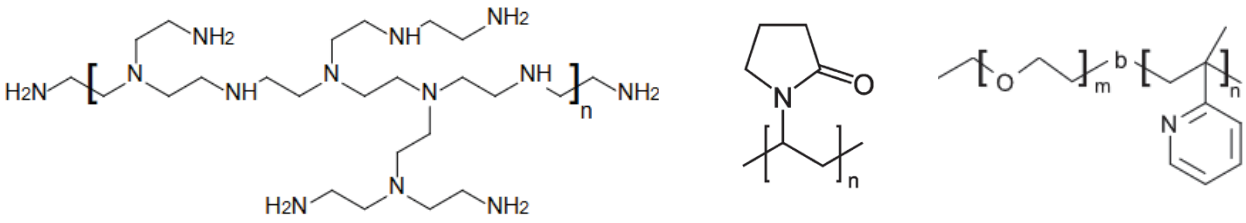

Figure 1. Molecular structure of the stabilizing polymers: branched polyethyleneimine (left), polyvinylpyrrolidone (middle) and poly(ethylene oxide)-*b*-poly(2-vinyl pyridine) (right).

Table 1. Molecular characteristics of the stabilizing polymers.

Polymer	M_n (g.mol^{-1})	M_w/M_n
PEI	25000	2.5
PVP	40000	2.0
PEO-*b*-P2VP	21000-*b*-13500	1.1

The proteins bovine serum albumin (BSA), immunoglobulin G from bovine serum (IgG) and lysozyme from chicken egg white were also purchased from Sigma-Aldrich under the catalog numbers A7030, I5506 and L6876, respectively.

Manufacturing of the Polymer-Stabilized AgNPs

The manufacturing of the AgNPs was conducted based on standard protocols reported in the literature and using sodium borohydride (NaBH4) for reducing Ag^{+} to Ag^{0}. [32,33] Briefly, aqueous solutions of $NaBH_4$ and $AgNO_3$ (1.0 mol.L-1) as well as polymer stock solutions were prepared. Aliquots of the stock $NaBH_4$ solution were added dropwise under stirring into $AgNO_3$/polymer solutions. The reaction mixtures were stirred vigorously until the complete addition of $NaBH_4$ and further stirred for 1h. The formation of AgNPs was noticed by the appearance of a characteristic pale yellow color. The remaining reactants were further removed by dialysis against pure water for 24h using a ready-to-use Spectra-Por® Float-A-Lyzer® G2 dialysis device with MWCO 100 kDa. Afterwards, the quantification (determination of molar concentration of AgNPs in each sample) has been performed as detailed hereafter.

Behavior in Protein Environments

The stability of the nanoparticles in aqueous media (0.15 $mol.L^{-1}$ NaCl with pH adjusted to 7.4 ± 0.2) has been investigated by placing them in contact with the model proteins BSA, IgG and lysozyme. The changes in size and UV-Vis profile were monitored as a function of protein concentration up to 5.0 $\mu mol.L^{-1}$ (respectively 0.3 $mg.mL^{-1}$, 0.8 $mg.mL^{-1}$ and 0.1 $mg.mL^{-1}$ for BSA, IgG and lysozyme). The molar concentration of each protein required to cover the produced AgNPs was estimated by firstly calculating the average surface area of each polymer-stabilized AgNPs as:

$$A_{Surface} = 4\pi R^2_{H-AgNPs} \quad (1)$$

Afterwards, the estimated number of protein molecules required to cover the whole surface of the assemblies (*N*) was computed as:

$$N = \frac{4R^2_{H-AgNPs}}{R^2_{H-Protein}} \quad (2)$$

These data are given in the Supporting Information File (Tables S1-S3).

Furthermore, the thermodynamics of protein-nanoparticle interaction was probed by isothermal titration calorimetry (ITC) and fluorescence spectroscopy data were acquired to evaluate quenching phenomena.

Methods

Dynamic Light Scattering (*DLS*): DLS measurements were performed using an ALV/CGS-3 compact goniometer system consisting of a 22 mW HeNe linearly polarized laser operating at a wavelength of 633 nm, an ALV 7004 digital correlator and a pair of avalanche photodiodes operating in pseudo cross-correlation mode. The data were collected by using the ALV Correlator Control software and the averaged intensity autocorrelation functions (based on 3 independent runs of 60s counting time) were subsequently analyzed using the algorithm REPES (incorporated in the GENDIST program) which employs the inverse Laplace transformation. The resulting distributions of relaxations times were evidenced to be monomodal (discussed hereafter) thereby allowing the further use the Cumulant method to estimate the polydispersity indexes as [34]:

$$\ln C(t) = \ln A - \Gamma t + \frac{\mu_2}{2} t^2 .... \quad (3)$$

where A is the amplitude of the autocorrelation function, Γ is the relaxation frequency (τ^{-1}) and the parameter μ_2 is known as the second-order cumulant. The hydrodynamic radius (R_H) of the nanoparticles was determined by using the Stokes-Einstein relation with $D = \tau^{-1} q^{-2}$:

$$R_H = \frac{k_B T q^2}{6\pi\eta} \tau \quad (4)$$

k_B is the Boltzmann constant, T is the absolute temperature, q is the scattering vector, η is the viscosity of the solvent (water) and τ is the mean relaxation time related to the diffusion of the nanoparticles. The polydispersity index of the samples (PDI) was computed as PDI = μ_2/Γ^2.

Electrophoretic Light Scattering (*ELS*): ELS measurements were used to determine the average zeta potential (ζ) of the polymer-stabilized silver colloids. The values were collected using a Zetasizer Nano-ZS ZEN3600 instrument (Malvern Instruments, UK). This instrument measures the electrophoretic mobility (U_E) and converts the value to ζ-potential (mV) through Henry's equation:

$$U_E = \frac{2 \varepsilon \zeta f(ka)}{3 \eta} \quad (5)$$

where □ is the dielectric constant of the medium (water) and η its viscosity with $f(ka)$, the Henry's function, calculated through the Smoluchowski approximation - $f(ka) = 1.5$.

Transmission Electron Microscopy (*TEM*)*:* The TEM samples were prepared by evaporating 5 drops (4 μL) of the colloidal materials into copper grids (400 square

mesh) coated with formvar. The micrographs were acquired with a JEOL JEM 1011 electron microscope operating at 100 kV.

UV-Vis Spectroscopy: UV-vis spectroscopy data were acquired by using a Thermo Scientific Evolution 201. The spectral resolution for wavelength scanning was 1.0 nm. The measurements were performed by using a quartz cell with optical path length of 10 mm.

Isothermal Titration Calorimetry (ITC): The thermodynamic parameters of protein-nanoparticle interaction were determined by isothermal titration calorimetry (ITC) performed at 25 ^{o}C using a MicroCal iTC200 Malvern calorimeter. The reference cell was filled with water, the sample cell was filled with 280 μL of polymer-stabilized AgNPs and the syringe was filled with the protein solutions. The titrations were performed by injecting 0.5 μL of protein solution in the sample cell every 150s. The raw data were integrated from a baseline to give the heat per injection as a function of the protein-to-nanoparticle ratio. The heat of dilution of the protein solutions was negligible as determined in blank experiments where the protein solutions were injected into the sample cell containing only the solvent. The resulting data were fitted whenever possible with the straightforward one-site model which assumes one site of nanoparticle-ligand interaction with a molar enthalpy (ΔH), stoichiometry of binding (N) and equilibrium association constant K. The changes in free energy (ΔG) and entropy (ΔS) associated with the process were obtained from fundamental thermodynamic relations ($\Delta G = -$ RT ln K = $\Delta H - T\Delta S$).

Fluorescence Spectroscopy: The fluorescence spectra were recorded on a Varian Cary Eclipse fluorescence spectrophotometer with excitation and emission slits placed at 90°. The apparatus is equipped with a Xe flash lamp to provide the excitation radiation. The selected excitation wavelength was 280 nm and the fluorescence emission was monitored in the range 300-450 nm after progressive additions of AgNPs into protein solutions. The measurements were acquired using a quartz cell with 10.0 mm optical path. The quenching mechanism was further evaluated whenever possible by fitting the Stern-Volmer equation as:

$$\frac{F_0}{F} = 1 + K_{SV}[\text{AgNPs}] \tag{6}$$

where F_0 and F are the values of fluorescence intensity of BSA in the absence and in the presence of different concentrations of AgNPs [AgNPs].

RESULTS AND DISCUSSION

Synthesis and Structural Features of the Polymer-Stabilized Silver Nanocolloids

The synthesis of the polymer-stabilized AgNPs was conducted upon dropwise addition of a previously prepared $NaBH_4$ solution into polymer/$AgNO_3$ solutions followed by vigorous stirring for 1h. The procedure is cartooned in Figure 2(a).

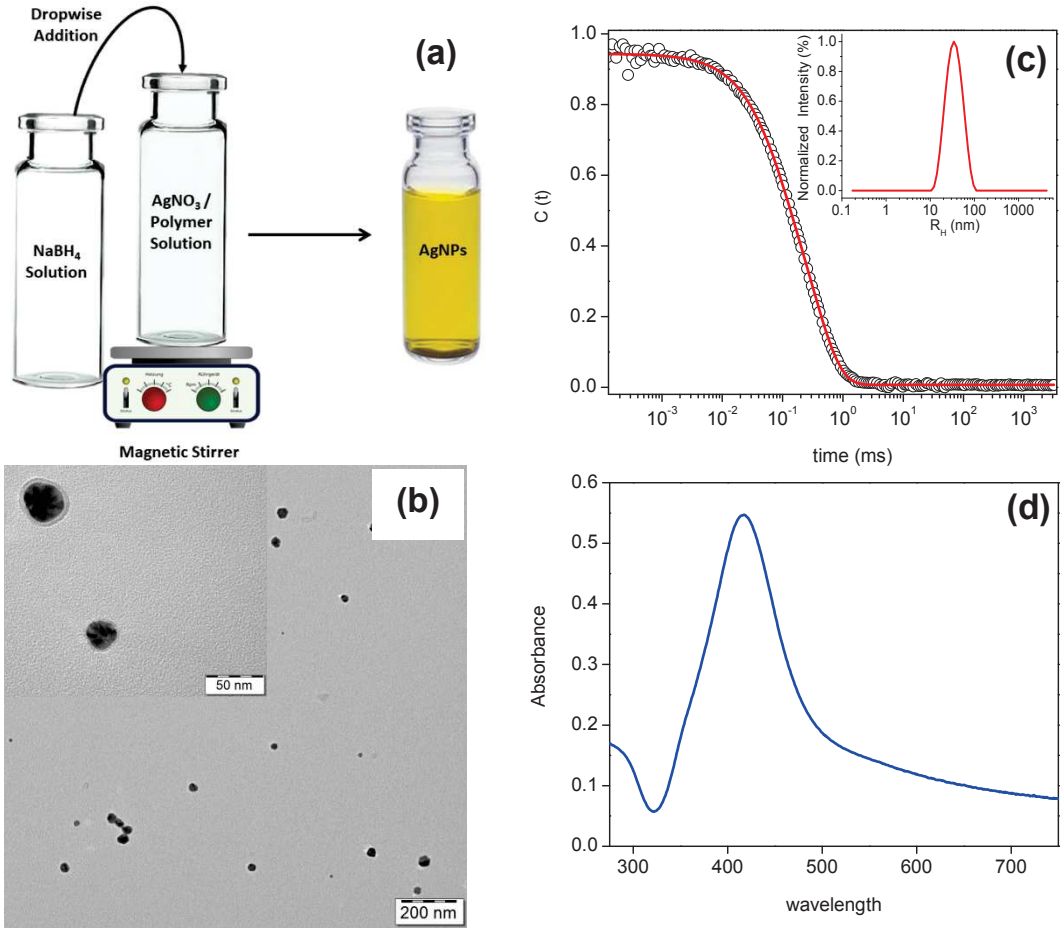

Figure 2. Schematic representation of the procedure used to prepare the polymer-stabilized AgNPs (a) and characterization of the AgNPs@PEI by transmission electron microscopy - TEM (b), autocorrelation curve obtained by dynamic light scattering and respective distribution of R_H - inset (c) and UV-Vis absorbance spectrum (d).

The prompt appearance of the characteristic pale yellow color upon mixing the starting solutions is the fingerprint related to the formation of nano-sized silver colloids. Subsequently, the remaining staring materials (ions and/or polymer chains) were removed by dialysis for 24h.

The prepared polymer-stabilized AgNPs were characterized by a variety of techniques: dynamic (DLS) and electrophoretic (ELS) light scattering, UV-Vis spectroscopy and transmission electron microscopy (TEM). In the Figure 2, it is portrayed the whole set of experimental data regarding the characterization of the PEI-stabilized AgNPs (AgNPs@PEI). The same procedure has been applied to characterize the other polymer-stabilized AgNPs and the structural parameters obtained are summarized in Table 2.

Table 2. Structural Parameters of the manufactured polymer-stabilized AgNPs.

Polymer Capping	R_H (nm)	ζ (mV)	PDI	λ_{max} (nm)
PEI	32.4	+ 13.0	0.45	415.2
PVP	32.4	- 12.7	0.44	403.0
PEO-*b*-P2VP	33.0	+15.6	0.40	420.0

The hydrodynamic size of the obtained hybrid polymer-stabilized AgNPs are reasonably similar (R_H ~ 32-33 nm). The representative TEM image for AgNPs@PEI portrayed in Figure 2(b) clearly demonstrates the silver core stabilized by a thin polymer layer. This can be observed also for AgNPs@PVP, and particularly for AgNPs@PEO-*b*-P2VP as reported in the Supporting Information File (Figure S1). The employed protocol conducted to monomodal distributions of AgNPS such as representatively portrayed in Figure 2c. Nevertheless, the prepared silver colloids are polydisperse (PDI > 0.15) regardless the chemical nature of the stabilizer. The ζ-

potential values reflect the chemical characteristics of the polymer shells where PEO-*b*-P2VP and PEI-stabilized AgNPs hold a positive surface charge whereas a negatively charged surfaces was monitored for PVP-stabilized AgNPs. The residual surface charges are probably the consequence of different charge partitioning and-or configuration of the polymer chains at the interface.

The investigations regarding the behavior in protein environments were preceded by the estimation of AgNPs molar concentration (C_{AgNPs}) in each sample. Accordingly, C_{AgNPs} values for the silver colloids were estimated using the Lambert-Beer law taking into account the measured absorbance at λ_{max} (A_{max}) as:

$$C_{AgNPs} = \frac{A_{max}}{\varepsilon\, b} \tag{7}$$

The respective value for the extinction molar coefficient (□) was selected considering the average size and λ_{max} of each produced AgNPs as based on the tabulated reference data-set proposed by Paramelle et al. [35]. The optical path (*b*) was equal to 10 mm. The same protocol has been applied recently by us and the results were in reasonable agreement compared to ICP-OES determinations.[36] The Table 3 reports the literature values and experimental data, as well as the determined amounts of AgNPs (molar concentrations) at each starting AgNPs stock solution. The corresponding *m*/*v* concentrations are also provided. They were determined as described in details elsewhere.[36]

Table 3. Summary of parameters used for determining the molar concentrations of AgNPs based on UV-Vis spectra.

Polymer Capping	$A_{\lambda max}$	λ_{max} (nm)	ε (10^8 $M^{-1}cm^{-1}$)	[AgNPs] 10^{-11} M	[AgNPs] $\mu g.mL^{-1}$
PEI	0.629	415.2	416	1.5	4.3
PVP	0.349	403.0	90.5	3.9	2.2
PEO-*b*-P2VP	0.261	420.0	537	0.5	2.0

The values given in Table 3 reveal concentrations in the range ~ 10^{-11} $mol.L^{-1}$. These stock solutions were normalized by dilution to an equal starting concentration in order to further probe the behavior of the nano-sized silver colloids in different protein environments.

Behavior in Protein Environments

Taking into account that data given in the Supporting Information File (Tables S1-S3) and the molar concentrations reported in Table 3, it has been monitored R_H as a function of protein concentration at least up the values required to cover the whole surface of the assemblies. The results are shown and discussed below.

AgNPs@PEI in Protein Environments

The Figure 3 (left) portrays the UV-vis spectra for AgNPs@PEI as a function of increased BSA (A), IgG (B) and lysozyme (C) concentrations. The respective autocorrelation functions measured by DLS at same concentration ranges are given in the right.

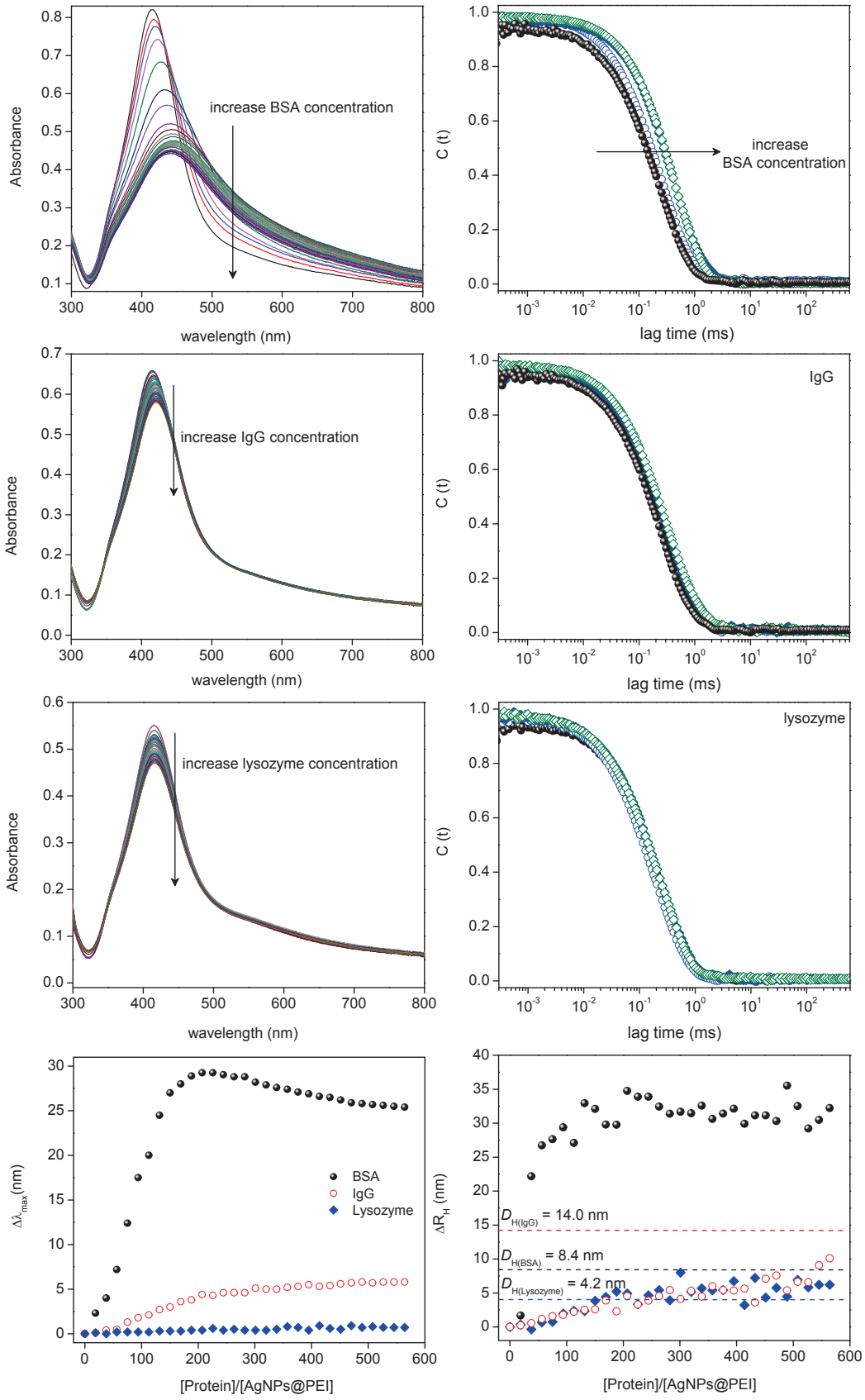
Absorbance
wavelength (nm)
increase BSA concentration
C (t)
lag time (ms)
increase
BSA concentration
increase IgG concentration
IgG
increase lysozyme concentration
lysozyme
BSA
IgG
Lysozyme
[Protein]/[AgNPs@PEI]
$D_{H(IgG)}$ = 14.0 nm
$D_{H(BSA)}$ = 8.4 nm
$D_{H(Lysozyme)}$ = 4.2 nm

Figure 3. UV-Vis spectra (left) for AgNPs@PEI monitored as a function of increased amounts of protein concentration in different model environments according to the legends, and analogous autocorrelation functions (right). The values of $\Delta\lambda_{max}$ (left) and ΔR_H (right) as a function of [protein]/[AgNPs@PEI] are given at the bottom.

The UV-vis profiles of all investigated pure proteins at relatively high concentration are provided in the Supporting Information File (Figure S2).They evidence that the pure proteins do not have any remarkable visible light absorption close to ~ 400 nm which is the region of the AgNPs absorption band. Indeed, remarkable differences can be noticed in the profiles for AgNPs@PEI in BSA environment. The most important information regarding such data is the shift of λ_{max} towards higher wavelengths as BSA concentration increases. This points out that BSA adsorption is taking place at the surface of BPEI-stabilized AgNPs as also validated by the shift towards the right-hand side of the main decay of the autocorrelation functions reported in Figure 3 (right) in BSA environment. Although remaining PEI is presumably absent after dialysis, the intermolecular interaction between the free chains and BSA can also occur as evidenced by isothermal titration calorimetry (Figure S3a). Nevertheless, the SPR absorption band is a fingerprint linked to the existence of silver colloids and the changes observed can only be related to changes at their surfaces whereas the interaction between BSA and free PEI chains cannot be seen by UV-vis at $\lambda \sim 400$ nm (Figure S3b). Besides, the size of free PEI/BSA aggregates ($R_H \sim 160$ nm) is remarkably larger than the size of the PEI-coated AgNPs before ($R_H \sim 30$ nm) or after ($R_H \sim 55$ nm) protein adsorption (Figure S3c). Therefore, these data robustly confirm that the interactions observed are necessarily taking place at the surface of the nanoparticles. Additionally, the DLS data for free PEI/BSA is highly relevant because it

suggests negligible amount of free chains at the system after dialysis since such huge aggregates have not been observed at the AgNPs-containing samples.

The values of λ_{max} and R_H as a function of [protein]/[AgNP@sPEI] are given at the bottom of Figure 3 where it can be noticed that the size of the assemblies increase pronounced as soon as small amounts of BSA are present. Afterwards, it remains essentially constant. The size increases by about ~ 30 nm in BSA environment therefore clearly suggesting protein-nanoparticle interaction. Indeed, ΔR_H is noticeably bigger than the diameter of BSA ($D_{H\text{-}BSA}$ = 8.4 nm) and therefore, the experimental data suggest the development of a multilayered protein shell. The protein adsorption is also suggested by the changes in the UV-vis profile where the red shift points out increasing in the nanoparticle's size. The reduction in UV-vis absorption ($A_{\lambda max}$) might be related to the dilution due to the addition of increased aliquots of the BSA solution, however, taking into account the Lambert-Beer law and the linear dependence of the AgNPs concentration with regard to $A_{\lambda max}$, the reduction is mainly related to changes in the hybrid material. On the other hand, the behavior in IgG and lysozyme environments are considerably different. The reduction in $A_{\lambda max}$ in both cases can be wholly attributed to the dilution inherent to the employed protocol of titration. In these cases, a reduction of $A_{\lambda max}$ by about ~ 13% is expected. The λ_{max} of the produced AgNPs in lysozyme environment remained roughly constant. Indeed, in such a case, the value of ΔR_H at the end of the titration is nearly equal to the diameter of lysozyme ($D_{H\text{-}Lysozyme}$ = 4.2 nm) however, since this is a fairly small protein molecule as compared to the size of the AgNPs@PEI, such increase was evidenced to be still within the experimental errors of R_H determination. Accordingly, these data in principle suggest that protein adsorption is not taking place as also confirmed by other sets of measurements (discussed hereafter). The behavior in IgG environment is not remarkably different, however, in such a case, a

slight displacement of λ_{max} towards higher wavelengths is noticed ($\Delta\lambda \sim 5$ nm). Nevertheless, the increased size (ΔR_H) is not compatible with the development of a IgG monolayer around the AgNPs (which would lead to $\Delta R_H \sim 14$ nm according to the diameter of the IgG molecule which is a fairly large protein). Taking together, the DLS and UV-vis data agree and confirm robustly only the BSA adsorption onto the surface of the PEI-stabilized AgNPs. On the other hand, they suggest that IgG and lysozyme adsorption in principle do not occur. Presumably, the small changes in λ_{max} in the IgG environment are related to changes in the surroundings of the metallic colloids.

The investigations regarding the protein adsorption around AgNPs@PEI was further complemented by fluorescence spectroscopy measurements. This technique is useful to evaluate nanoparticle-protein binding since the phenomenon may quench the fluorescence of tryptophan, tyrosine and phenylalanine residues, for instance.[37] The Figure 4 portrays the fluorescence spectra of BSA, lysozyme and IgG at the presence of increased amounts of AgNPs@PEI according to the legends.

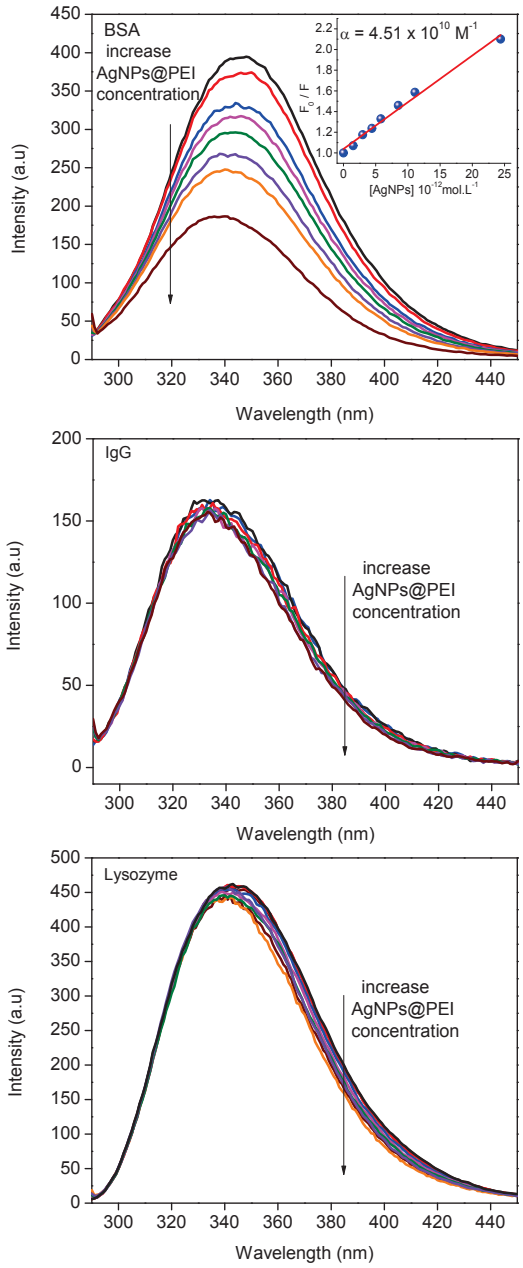

Figure 4. Fluorescence spectra of proteins and fluorescence quenching of BSA caused by the addition of successive aliquots of AgNPs@PEI - inset**:** Stern-Volmer plot for the fluorescence quenching of BSA by AgNPs@PEI (T = 296 K; λ_{ex} = 280 nm, concentration range of AgNPs@PEI: 0 - 5.0 x 10^{-12} M)**.**

The data agree very well with the DLS and UV-Vis results reported and discussed previously. The quenching phenomenon is clearly visible only when BSA is

in contact with AgNPs@PEI since the fluorescence emission intensity of the protein is gradually reduced as a function of AgNPs@PEI concentration. This data undoubtedly confirm that protein-nanoparticle intermolecular interactions are taking place. Additionally, there can be seen a slight shift in the maximum emission wavelength towards smaller values suggesting changes in the polarity of the microenvironment around the fluorescent residues of BSA. On the other hand, the presence of AgNPs@PEI does not quench lysozyme and IgG fluorescence thereby suggesting once again that protein adsorption is not taking place for such pairs. The quenching mechanism was further evaluated by fitting the Stern-Volmer equation (Equation 6). The experimental data and respective curve fitting are given as an inset in Figure 4. The very good Stern-Volmer plot linearity suggests the dominance of one single quenching mechanism. The determined Stern-Volmer constant (K_{SV} = 4.51 x 10^{10} M^{-1}) and the further calculated value of the quenching rate constant ($K_b = K_{SV} / \tau_0$ with $\tau_0 \sim 10^{-8}$ s^{-1}) [38] leads to a value much higher (K_b = 4.51 x 10^{18} M^{-1}) than the value for threshold diffusion collision rate constant of quenchers to proteins (2×10^{10} $M^{-1}s^{-1}$).[39,40] This accordingly points out the formation of ground-state complexes and therefore the quenching mechanism is static highlighting the actual protein-nanoparticle interaction.

In the step further, ITC measurements were performed and the data are provided in Figure 5.

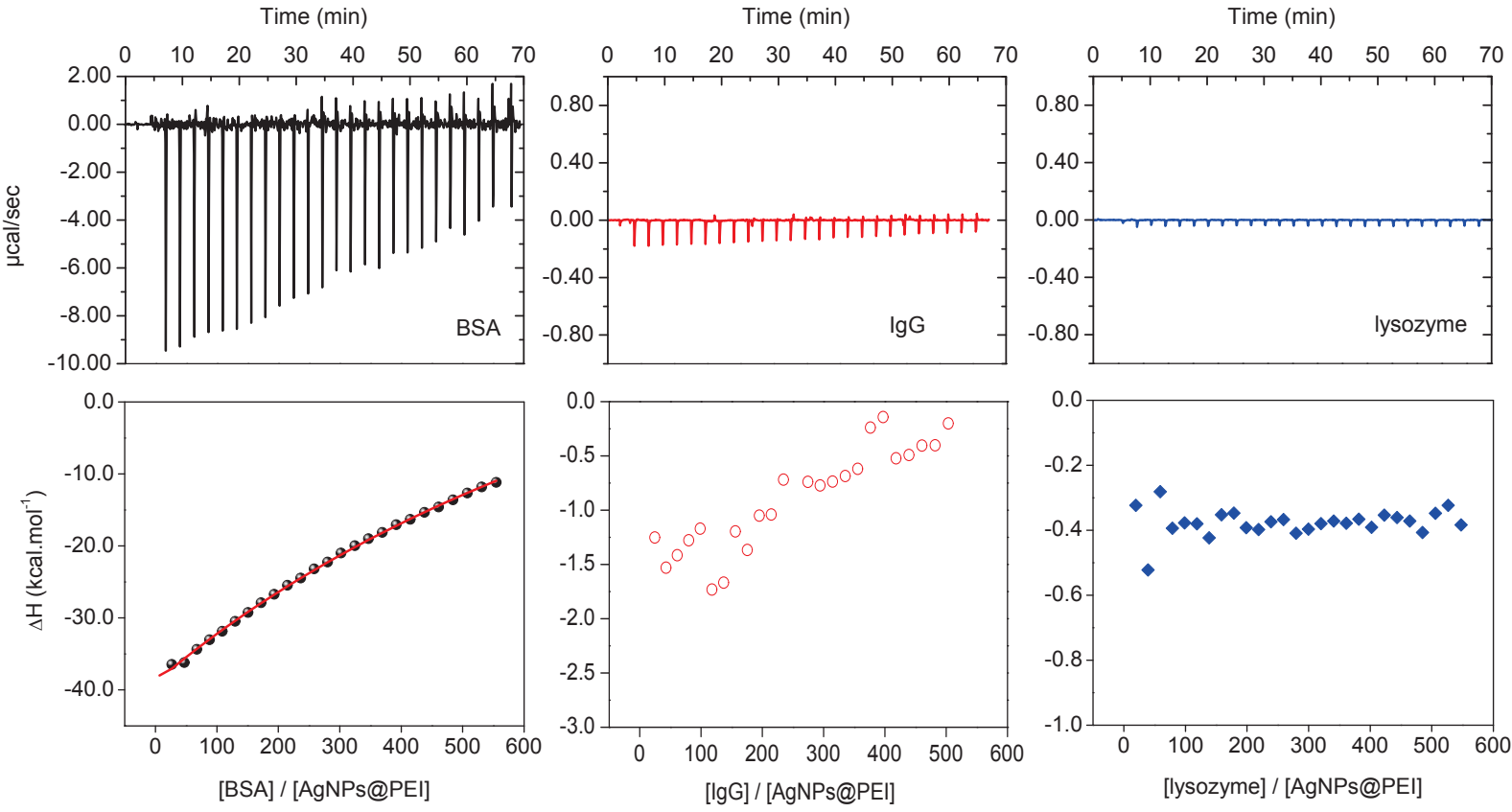

Figure 5. ITC raw data for the titration of BSA, lysozyme and IgG into AgNPs@PEI and respective values of energy per mol of injected protein according to the legends.

Particularly regarding the pair BSA-AgNPs@PEI, the raw ITC data clearly demonstrate that the BSA adsorption is an exothermic process. The values of heating rates are negligible for lysozyme-AgNPs@PEI and IgG-AgNPs@PEI as compared to the titration using BSA. The experimental data could be fitted by using the straightforward one-site binding model. Accordingly, the molar enthalpy (ΔH), stoichiometry of binding (N) that is, the number of protein molecules per nanoparticle and the equilibrium association constant K_A for the adsorption of BSA onto the AgNPs@PEI were obtained. Furthermore, the molar free energy change (ΔG) and the molar entropy change (ΔS) of the binding event were determined *via* fundamental thermodynamic equations. The fitting parameters obtained were respectively - 39

kcal.mol^{-1}, 3.4 x 10^{6} M^{-1} and 446 for ΔH, K_A and N. The calculated values for ΔS and ΔG were respectively equal to - 101 cal.mol^{-1}.K^{-1} and - 8.9 kcal.mol^{-1}. The value of N evidences that approximately 450 BSA molecules bind to each AgNPs@PEI. This value is nearly twice large than the required for theoretical complete coating of the produced metallic colloids. To some extent, the result is compatible to the large increase in R_H reported for such system in BSA environment. Moreover, the signals of the thermodynamic parameters can be used to identify the prevalence of electrostatic, hydrophobic, hydrogen bonding or van der Waals interactions. The dominance of hydrophobic effects can be ruled out since this is assigned for endothermic and entropically-driven processes ($\Delta H > 0$ and $\Delta S > 0$). On the other hand, the prevalence of electrostatic interactions can be considered for exothermic events with positive variation of entropy ($\Delta H < 0$ and $\Delta S > 0$) whereas exothermic events with negative variation of entropy ($\Delta H < 0$ and $\Delta S < 0$) are observed when van der Walls and hydrogen bonding are the main operating forces. Accordingly, the fitting result suggests that the protein adsorption is mainly driven by van der Waals and hydrogen bonding [41–43] with the event leading to conformation restrictions and-or loss of rotational freedom thereby resulting in $\Delta S < 0$. Although the previous data (UV-Vis, DLS and fluorescence spectroscopy) already robustly confirmed the absence of lysozyme and IgG adsorption onto the surface of the AgNPs@PEI, we report the ITC also for such pairs in Figure 5. As mentioned before, the negligible heat transfers monitored suggest the absence of protein adsorption, as expected. Overall, there is a very good agreement between all the analytical techniques used to probe the protein adsorption onto the surface of the AgNPs@PEI hybrid colloids.

AgNPs@PVP in Protein Environments

The same investigations were performed for PVP-stabilized AgNPs (AgNPs@PVP) and the most relevant results are summarized in the panel Figure 6. Supplementary data are provided in Figures S4-S5 (Supporting Information file).

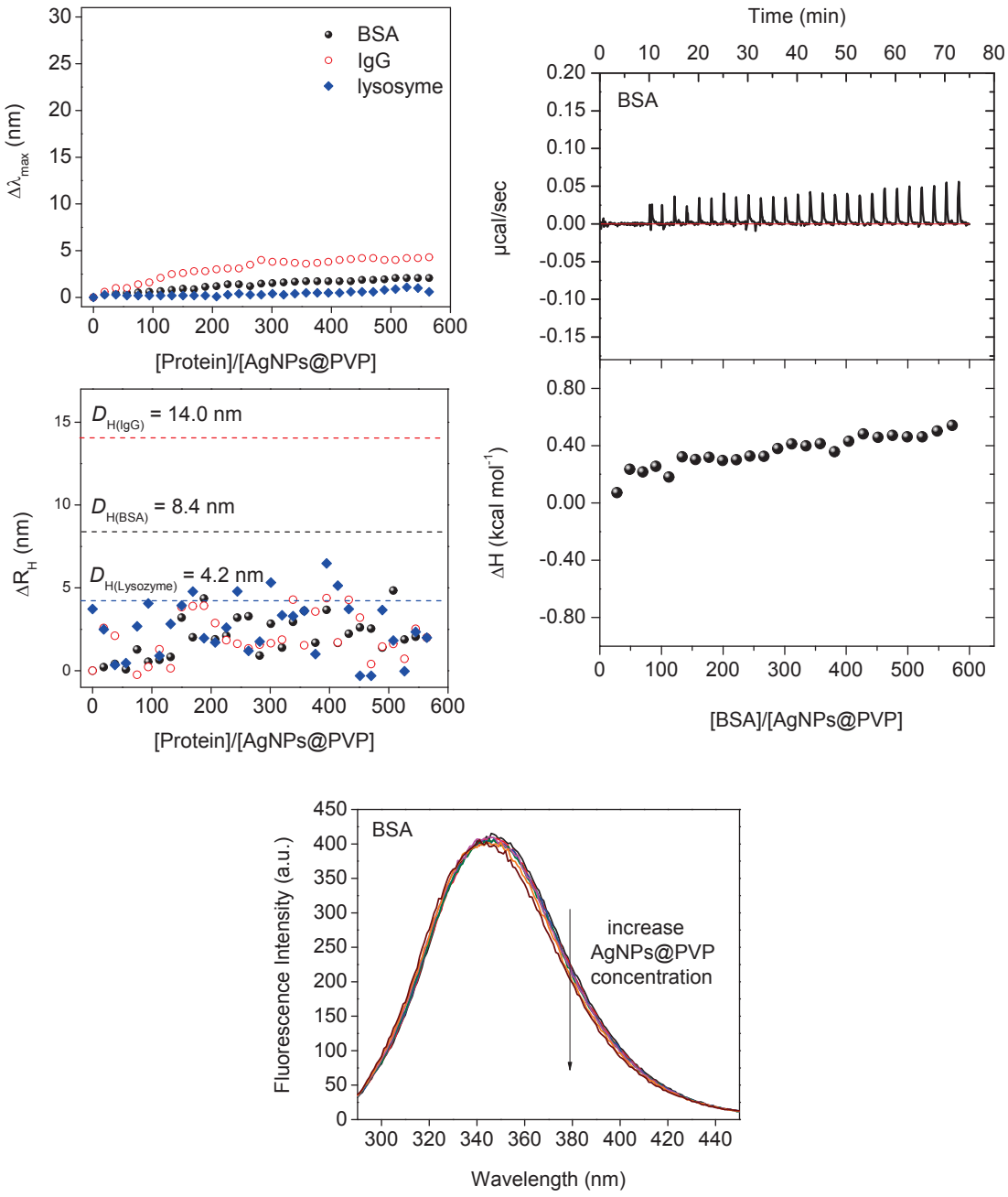

Figure 6. (Left) Values of $\Delta\lambda_{max}$ and ΔR_H as a function of [protein]/[AgNPs@PVP], (Right) ITC raw data and respective values of energy per mol of injected protein as a function of protein-to-nanoparticle ratio for the titration of BSA into AgNPs@PVP, (Bottom) Fluorescence spectra of BSA in the presence of different concentrations of AgNPs@PVP (T = 296 K; λ_{ex} = 280 nm; concentration range of AgNPs@PVP: 0 - 5.0 x 10^{-12} M)**.**

The experimental data are remarkably different than those monitored for AgNPs@PEI. They evidence that the presence of BSA essentially does not affect λ_{max} and size of the prepared AgNPs@PVP. The behavior is similar in lysozyme and IgG environments since the values of $\Delta\lambda_{max}$ and ΔR_H *vs*. [protein]/[AgNPs@PVP] remain nearly constant. These data suggest the outstanding property of PVP as stabilizer and protein-repelling shell for the produced silver colloids. Indeed, the behavior of $\Delta\lambda_{max}$ in IgG environment is almost identical to the one observed for PEI-stabilized AgNPs suggesting that the small increase in ($\Delta\lambda_{max}$ ~ 5 nm) is not linked to protein-nanoparticle interaction. The values of $\Delta\lambda_{max}$ in lysozyme and BSA environments are close to zero. The values of ΔR_H corroborate the UV-Vis data and they are never larger than the dimension of the protein molecules thereby once again suggesting the protein layers are not developed around the PVP-stabilized AgNPs. The values of ΔR_H at lysozyme environment oscillate in the range (0-5 nm). Nevertheless, considering the UV-Vis data and the oscillating behavior, presumably the observed changes are just within experimental errors of R_H determination thereby does not suggesting protein adsorption. Truly, the absence of nanoparticle-protein interactions was further confirmed by using fluorescence and isothermal titration calorimetry measurements since protein fluorescence quenching has not been detected and only negligible values

of heat transfer (ITC) were monitored. This is representatively portrayed for BSA environment in Figure 6. The data for lysozyme and IgG environments are given in the Supporting Information File (Figure S5).

AgNPs@PEO-b-P2VP in Protein Environments

The DLS and UV-Vis data for PEO-*b*-P2VP stabilized AgNPs in protein environments are provided in Figure 7 and S6. They are essentially the same regardless protein chemical nature and concentration since neither $\Delta\lambda_{max}$ nor the dimension of the hybrid material (R_H) are remarkably affected by the presence of the biomacromolecules. The results accordingly suggest notable stability of such assemblies in protein environments without evidences of protein adsorption and-or aggregation.

The outstanding protein-repelling characteristic of poly(ethylene-oxide) is quite well known, although it depends on polymer conformation and chain length. In the current case, the long PEO chain is probably above the minimum to get full stabilization property for the synthesized AgNPs. Indeed, it has been previously observed that $M_{w(PEO)} \sim 5000$ g.mol^{-1} is needed to provide silica nanoparticles with improved colloidal stabilization and almost no interaction with BSA or lysozyme whereas shorter chains are not able to repel proteins of different chemical nature.[44] Presumably, due to the hydrophobic character of P2VP, the block is closer to the silver (Ag^0) nuclei, and the hybrid metallic-organic core is then stabilized by the PEO hydrophilic shell. This arrangement seems to conduct to highly stable and protein-repelling structures. Indeed, the large molecular weight of PEO (21000 g.mol^{-1}) avoids effectively the protein adsorption onto the surface of the polymer-stabilized AgNPs.

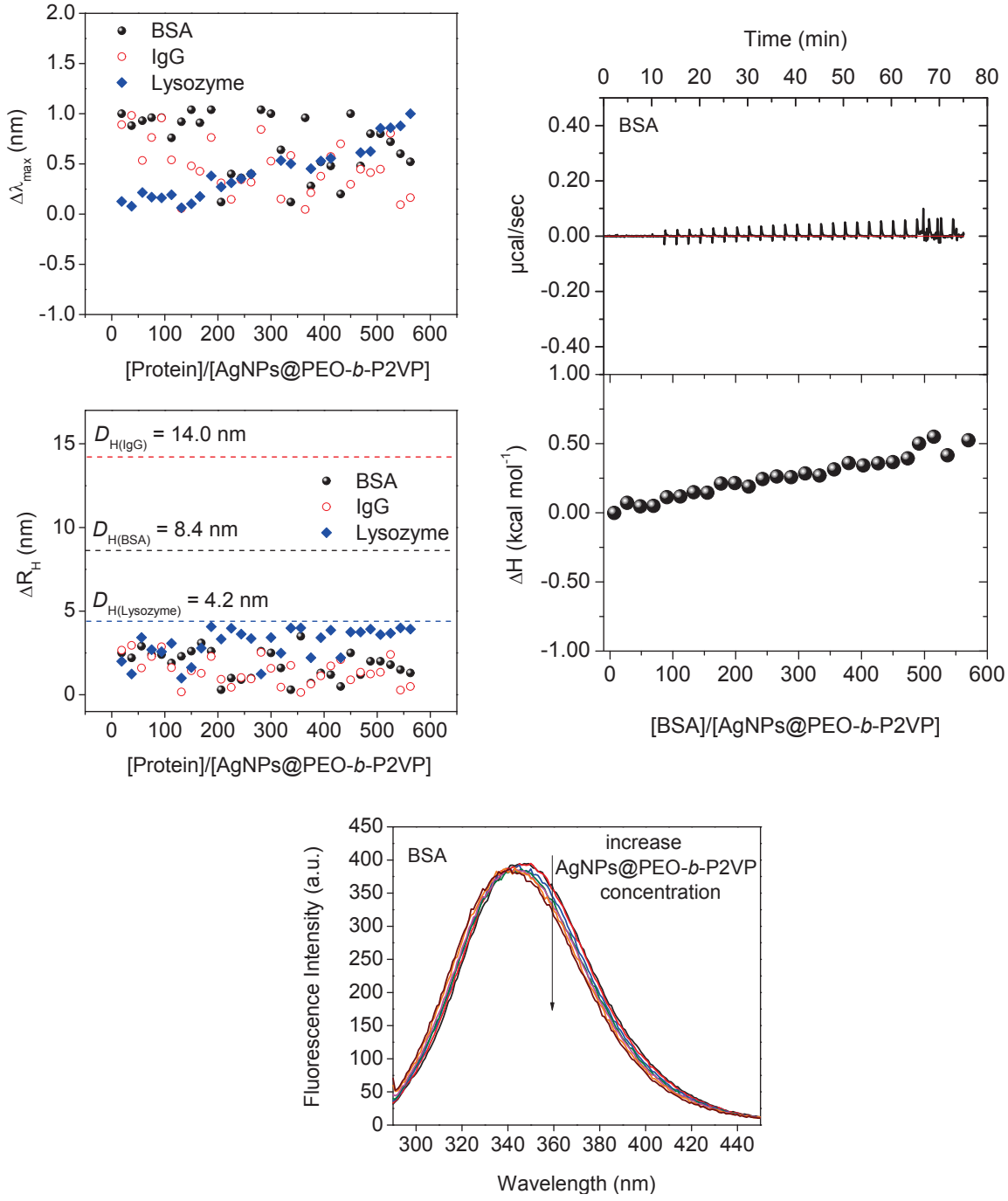

Figure 7. (Left) Values of $\Delta\lambda_{max}$ (top) and ΔR_H (bottom) as a function of [protein]/[AgNPs@PEO-*b*-P2VP], (Right) ITC raw data and respective values of energy per mol of injected protein as a function of protein-to-nanoparticle ratio for the titration of BSA into AgNPs@PEO-*b*-P2VP, (Bottom) Fluorescence spectra of BSA in the presence of different concentrations of AgNPs@PEO-*b*-P2VP (T = 296 K; λ_{ex} = 280 nm; concentration range of AgNPs@PEO-*b*-P2VP: 0 - 5.0 x 10^{-12} M).

The protein-repelling feature of AgNPs@PEO-*b*-P2VP has been further confirmed by ITC and fluorescence spectroscopy measurements since nor fluorescence quenching neither energy transfer for titration of proteins onto the polymer-stabilized silver colloid has been observed. These data are reported in Figure 7 and S7 (Supporting Information File).

CONCLUSIONS

We investigated the protein adsorption onto the surface of polymer-stabilized AgNPs. The results highlight that PEO-*b*-P2VP and PVP-stabilized AgNPs are resistant to BSA, IgG and lysozyme adsorption. The AgNPs coated by PEI are stable in IgG and lysozyme environments however, BSA adsorption has been clearly evidenced. In such a case, the protein adsorption is mainly driven by van der Waals and hydrogen bonding as suggested by isothermal titration calorimetry. Accordingly, polymer coatings can provide protein-repelling features to metallic assemblies, depending on its chemical nature. These results diverge remarkably compared to those related to non-coated metallic assemblies which were evidenced to be very prone to protein adsorption. For instance, BSA adsorption was evidenced to take place at the surface of negatively charged citrate [45–47] and borohydride-stabilized [48] AgNPs. This has been similarly observed at the surface of citrate-stabilized AuNPs.[49] It thus seems to be a quite general phenomenon. Therefore, we consider these findings of due relevance towards the rational design of nanoparticles for biomedical applications. The manufacturing of assemblies resistant to protein adsorption will likely help them to preserve the biological activity while circulating in biological milieus possibly avoiding aggregation and fast clearance. Besides, the different behavior regarding protein adsorption is

supposed to impact the biotechnology applications of polymer-coated silver colloids. Nevertheless, we highlight the limitations of the current findings with respect to *in vivo* extrapolation of the experimental evidences: *i*) due to temporal stability concerns, the experiments have been conducted in isotonic media, while not buffered such as the plasma environment, *ii*) we have used protein concentrations suitable to satisfy the requirement of full nanoparticle coating and therefore, the amounts are significantly smaller than those found in the bloodstream, *iii*) although in model protein solutions PVP and PEO-coatings were evidenced to confer protein repelling feature in similar extents, the behavior *in vivo* can be remarkably different such as, for instance, previously evidenced for PLA-based nanoparticles.[50] The *in vivo* extrapolation of experimental observations is indeed highly complex, nonetheless, the evidenced high susceptibility of AgNPs@PEI to BSA adsorption may influence their biological activity. There are experiments underway concerning the effect of protein coronas around the same polymer-stabilized AgNPs with respect to their cytotoxicity, hemolytic behavior and biocide effects.

ACKNOWLEDGMENTS

These investigations were sponsored by FAPESP (Grant no. 2017/00459-4) and CNPq (400124/2016-5). C.C.S.B acknowledges the fellowships granted by FAPESP (Grant no.2017/24603-7 and 2019/03223-7). F.C.G acknowledges the fellowship granted by CNPq (Grant No. 302467/2014-9). The CEM at UFABC is acknowledged for providing accessibility to the Malvern light scattering instrument. A.J. and P.S. acknowledge the support of the Grant Agency of the Czech Republic (grant 20-13946Y) and of the Ministry of Education, Youth and Sports of CR within the National

Sustainability Program I (NPU I), Project POLYMAT LO1507. This project has also received funding from the European Union's Horizon 2020 research and innovation programme under the Marie Skłodowska-Curie grant agreement No 823883.

REFERENCES

[1] P. Ghosh, G. Han, M. De, C.K. Kim, V.M. Rotello, Gold nanoparticles in delivery applications, Adv. Drug Deliv. Rev. 60 (2008) 1307–1315. https://doi.org/10.1016/j.addr.2008.03.016.

[2] R.A. Sperling, P. Rivera Gil, F. Zhang, M. Zanella, W.J. Parak, Biological applications of gold nanoparticles, Chem. Soc. Rev. 37 (2008) 1896. https://doi.org/10.1039/b712170a.

[3] R.R. Arvizo, S. Bhattacharyya, R. a. Kudgus, K. Giri, R. Bhattacharya, P. Mukherjee, Intrinsic therapeutic applications of noble metal nanoparticles: past, present and future, Chem. Soc. Rev. 41 (2012) 2943. https://doi.org/10.1039/c2cs15355f.

[4] J.R. Morones, J.L. Elechiguerra, A. Camacho, K. Holt, J.B. Kouri, J.T. Ramírez, M.J. Yacaman, The bactericidal effect of silver nanoparticles, Nanotechnology. 16 (2005) 2346–2353. https://doi.org/10.1088/0957-4484/16/10/059.

[5] C. Marambio-Jones, E. Hoek, A review of the antibacterial effects of silver nanomaterials and potential implications for human health and the environment, J. Nanoparticle Res. 12 (2010) 1531–1551. https://doi.org/10.1007/s11051-010-9900-y.

[6] A. Panáček, M. Kolář, R. Večeřová, R. Prucek, J. Soukupová, V. Kryštof, P. Hamal, R. Zbořil, L. Kvítek, Antifungal activity of silver nanoparticles against

Candida spp., Biomaterials. 30 (2009) 6333–6340. https://doi.org/10.1016/j.biomaterials.2009.07.065.

[7] H. Guo, Z. Zhang, B. Xing, A. Mukherjee, C. Musante, J.C. White, L. He, Analysis of silver nanoparticles in antimicrobial products using surface-enhanced raman spectroscopy (SERS), Environ. Sci. Technol. 49 (2015) 4317–4324. https://doi.org/10.1021/acs.est.5b00370.

[8] C. Beer, R. Foldbjerg, Y. Hayashi, D.S. Sutherland, H. Autrup, Toxicity of silver nanoparticles-Nanoparticle or silver ion?, Toxicol. Lett. 208 (2012) 286–292. https://doi.org/10.1016/j.toxlet.2011.11.002.

[9] Z. Chen, P. Yang, Z. Yuan, J. Guo, Aerobic condition enhances bacteriostatic effects of silver nanoparticles in aquatic environment: An antimicrobial study on Pseudomonas aeruginosa, Sci. Rep. 7 (2017) 1–8. https://doi.org/10.1038/s41598-017-07989-w.

[10] a R. Gliga, S. Skoglund, I.O. Wallinder, B. Fadeel, H.L. Karlsson, Size-dependent cytotoxicity of silver nanoparticles in human lung cells: the role of cellular uptake, agglomeration and Ag release, Part Fibre Toxicol. 11 (2014) 11. https://doi.org/10.1186/1743-8977-11-11.

[11] K.J. Lee, P.D. Nallathamby, L.M. Browning, C.J. Osgood, X.-H.N. Xu, In Vivo Imaging of Transport and Biocompatibility of Single Silver Nanoparticles in Early Development of Zebrafish Embryos, ACS Nano. 1 (2007) 133–143. https://doi.org/10.1021/nn700048y.

[12] X. Zhang, M. Yao, M. Chen, L. Li, C. Dong, Y. Hou, H. Zhao, B. Jia, F. Wang, Hyaluronic Acid-Coated Silver Nanoparticles As a Nanoplatform for in Vivo Imaging Applications, ACS Appl. Mater. Interfaces. 8 (2016) 25650–25653. https://doi.org/10.1021/acsami.6b08166.

[13] M. Kopp, S. Kollenda, M. Epple, Nanoparticle-Protein Interactions: Therapeutic Approaches and Supramolecular Chemistry, Acc. Chem. Res. 50 (2017) 1383–1390. https://doi.org/10.1021/acs.accounts.7b00051.

[14] R. Gaspar, Nanoparticles: Pushed off target with proteins, Nat. Nanotechnol. 8 (2013) 79–80. https://doi.org/10.1038/nnano.2013.11.

[15] N. Durán, C.P. Silveira, M. Durán, D.S.T. Martinez, Silver nanoparticle protein corona and toxicity: a mini-review, J. Nanobiotechnology. 13 (2015) 55. https://doi.org/10.1186/s12951-015-0114-4.

[16] V. Gorshkov, J.A. Bubis, E.M. Solovyeva, M. V. Gorshkov, F. Kjeldsen, Protein corona formed on silver nanoparticles in blood plasma is highly selective and resistant to physicochemical changes of the solution, Environ. Sci. Nano. 6 (2019) 1089–1098. https://doi.org/10.1039/C8EN01054D.

[17] T. Miclăuş, C. Beer, J. Chevallier, C. Scavenius, V.E. Bochenkov, J.J. Enghild, D.S. Sutherland, Dynamic protein coronas revealed as a modulator of silver nanoparticle sulphidation in vitro, Nat. Commun. 7 (2016) 11770. https://doi.org/10.1038/ncomms11770.

[18] K. Saha, D.F. Moyano, V.M. Rotello, Protein coronas suppress the hemolytic activity of hydrophilic and hydrophobic nanoparticles, Mater. Horiz. 1 (2014) 102–105. https://doi.org/10.1039/C3MH00075C.

[19] C. Corbo, R. Molinaro, A. Parodi, N.E. Toledano Furman, F. Salvatore, E. Tasciotti, The impact of nanoparticle protein corona on cytotoxicity, immunotoxicity and target drug delivery, Nanomedicine. 11 (2016) 81–100. https://doi.org/10.2217/nnm.15.188.

[20] A. Salvati, A.S. Pitek, M.P. Monopoli, K. Prapainop, F.B. Bombelli, D.R. Hristov, P.M. Kelly, C. Åberg, E. Mahon, K.A. Dawson, Transferrin-

functionalized nanoparticles lose their targeting capabilities when a biomolecule corona adsorbs on the surface, Nat. Nanotechnol. 8 (2013) 137–143. https://doi.org/10.1038/nnano.2012.237.

[21] S. Tenzer, D. Docter, J. Kuharev, A. Musyanovych, V. Fetz, R. Hecht, F. Schlenk, D. Fischer, K. Kiouptsi, C. Reinhardt, K. Landfester, H. Schild, M. Maskos, S.K. Knauer, R.H. Stauber, Rapid formation of plasma protein corona critically affects nanoparticle pathophysiology, Nat. Nanotechnol. 8 (2013) 772–781. https://doi.org/10.1038/nnano.2013.181.

[22] S. Juling, A. Niedzwiecka, L. Böhmert, D. Lichtenstein, S. Selve, A. Braeuning, A.F. Thünemann, E. Krause, A. Lampen, Protein Corona Analysis of Silver Nanoparticles Links to Their Cellular Effects, J. Proteome Res. 16 (2017) 4020–4034. https://doi.org/10.1021/acs.jproteome.7b00412.

[23] A.E. Nel, L. Mädler, D. Velegol, T. Xia, E.M. V Hoek, P. Somasundaran, F. Klaessig, V. Castranova, M. Thompson, Understanding biophysicochemical interactions at the nano–bio interface, Nat. Mater. 8 (2009) 543–557. https://doi.org/10.1038/nmat2442.

[24] I. Lynch, K.A. Dawson, Protein-nanoparticle interactions, Nano Today. 3 (2008) 40–47. https://doi.org/10.1016/S1748-0132(08)70014-8.

[25] J. Piella, N.G. Bastús, V. Puntes, Size-Dependent Protein–Nanoparticle Interactions in Citrate-Stabilized Gold Nanoparticles: The Emergence of the Protein Corona, Bioconjug. Chem. 28 (2017) 88–97. https://doi.org/10.1021/acs.bioconjchem.6b00575.

[26] T. Cedervall, I. Lynch, S. Lindman, T. Berggård, E. Thulin, H. Nilsson, K. a Dawson, S. Linse, Understanding the nanoparticle-protein corona using methods to quantify exchange rates and affinities of proteins for nanoparticles., Proc. Natl.

Acad. Sci. U. S. A. 104 (2007) 2050–2055. https://doi.org/10.1073/pnas.0608582104.

[27] G. Maiorano, S. Sabella, B. Sorce, V. Brunetti, M.A. Malvindi, R. Cingolani, P.P. Pompa, Effects of Cell Culture Media on the Dynamic Formation of Protein−Nanoparticle Complexes and Influence on the Cellular Response, ACS Nano. 4 (2010) 7481–7491. https://doi.org/10.1021/nn101557e.

[28] E. Casals, T. Pfaller, A. Duschl, G.J. Oostingh, V. Puntes, Time evolution of the nanoparticle protein corona, ACS Nano. 4 (2010) 3623–3632. https://doi.org/10.1021/nn901372t.

[29] K.A. Gibney, I. Sovadinova, A.I. Lopez, M. Urban, Z. Ridgway, G.A. Caputo, K. Kuroda, Poly(ethylene imine)s as antimicrobial agents with selective activity, Macromol. Biosci. 12 (2012) 1279–1289. https://doi.org/10.1002/mabi.201200052.

[30] H.J. Lee, S.G. Lee, E.J. Oh, H.Y. Chung, S.I. Han, E.J. Kim, S.Y. Seo, H. Do Ghim, J.H. Yeum, J.H. Choi, Antimicrobial polyethyleneimine-silver nanoparticles in a stable colloidal dispersion, Colloids Surfaces B Biointerfaces. 88 (2011) 505–511. https://doi.org/10.1016/j.colsurfb.2011.07.041.

[31] C. Batista, L. Albuquerque, C. Ribeiro, C. de Castro, E. Miranda, I. Nantes, B. Albuquerque, M. Cardoso, F. Giacomelli, Nano-Sized Silver Colloids Produced and Stabilized by Amino-Functionalized Polymers: Polymer Structure-Nanoparticle Features and Polymer StructureGrowth Kinetics Relationships, J. Braz. Chem. Soc. 28 (2017) 1608–1618. https://doi.org/10.21577/0103-5053.20160295.

[32] S. Agnihotri, S. Mukherji, S. Mukherji, Size-controlled silver nanoparticles synthesized over the range 5-100 nm using the same protocol and their

antibacterial efficacy, RSC Adv. 4 (2014) 3974–3983. https://doi.org/10.1039/c3ra44507k.

[33] Q. Zhang, N. Li, J. Goebl, Z. Lu, Y. Yin, A systematic study of the synthesis of silver nanoplates: Is citrate a “magic” reagent?, J. Am. Chem. Soc. 133 (2011) 18931–18939. https://doi.org/10.1021/ja2080345.

[34] P. Štěpánek, Dynamic light scattering: the method and some applications, in: W. Brown (Ed.), Oxford Sci. Publ., Oxford, 1993.

[35] D. Paramelle, A. Sadovoy, S. Gorelik, P. Free, J. Hobley, D.G. Fernig, A rapid method to estimate the concentration of citrate capped silver nanoparticles from UV-visible light spectra, Analyst. 139 (2014) 4855. https://doi.org/10.1039/C4AN00978A.

[36] C.C.S. Batista, L.J.C. Albuquerque, I. de Araujo, B.L. Albuquerque, F.D. da Silva, F.C. Giacomelli, Antimicrobial activity of nano-sized silver colloids stabilized by nitrogen-containing polymers: the key influence of the polymer capping, RSC Adv. 8 (2018) 10873–10882. https://doi.org/10.1039/C7RA13597A.

[37] C. Hao, G. Xu, Y. Feng, L. Lu, W. Sun, R. Sun, Fluorescence quenching study on the interaction of ferroferric oxide nanoparticles with bovine serum albumin, Spectrochim. Acta - Part A Mol. Biomol. Spectrosc. 184 (2017) 191–197. https://doi.org/10.1016/j.saa.2017.05.004.

[38] S. Chakraborti, P. Joshi, D. Chakravarty, V. Shanker, Z.A. Ansari, S.P. Singh, P. Chakrabarti, Interaction of polyethyleneimine-functionalized ZnO nanoparticles with bovine serum albumin, Langmuir. 28 (2012) 11142–11152. https://doi.org/10.1021/la3007603.

[39] S. Chakraborty, P. Joshi, V. Shanker, Z.A. Ansari, S.P. Singh, P. Chakrabarti,

Contrasting effect of gold nanoparticles and nanorods with different surface modifications on the structure and activity of bovine serum albumin, Langmuir. 27 (2011) 7722–7731. https://doi.org/10.1021/la200787t.

[40] Q. Yang, J. Liang, H. Han, Probing the interaction of magnetic iron oxide nanoparticles with bovine serum albumin by spectroscopic techniques, J. Phys. Chem. B. 113 (2009) 10454–10458. https://doi.org/10.1021/jp904004w.

[41] P.D. Ross, S. Subramanian, Thermodynamics of Protein Association Reactions: Forces Contributing to Stability, Biochemistry. 20 (1981) 3096–3102. https://doi.org/10.1021/bi00514a017.

[42] G. Rabbani, M.J. Khan, A. Ahmad, M.Y. Maskat, R.H. Khan, Effect of copper oxide nanoparticles on the conformation and activity of β-galactosidase, Colloids Surfaces B Biointerfaces. 123 (2014) 96–105. https://doi.org/10.1016/j.colsurfb.2014.08.035.

[43] S. Afrin, Riyazuddeen, G. Rabbani, R.H. Khan, Spectroscopic and calorimetric studies of interaction of methimazole with human serum albumin, J. Lumin. 151 (2014) 219–223. https://doi.org/10.1016/j.jlumin.2014.02.028.

[44] S. Louguet, A.C. Kumar, N. Guidolin, G. Sigaud, E. Duguet, S. Lecommandoux, C. Schatz, Control of the PEO Chain Conformation on Nanoparticles by Adsorption of PEO- block -Poly(l-lysine) Copolymers and Its Significance on Colloidal Stability and Protein Repellency, Langmuir. 27 (2011) 12891–12901. https://doi.org/10.1021/la202990y.

[45] M. Wang, C. Fu, X. Liu, Z. Lin, N. Yang, S. Yu, Probing the mechanism of plasma protein adsorption on Au and Ag nanoparticles with FT-IR spectroscopy, Nanoscale. 7 (2015) 15191–15196. https://doi.org/10.1039/c5nr04498g.

[46] J.T. Tai, C.S. Lai, H.C. Ho, Y.S. Yeh, H.F. Wang, R.M. Ho, D.H. Tsai, Protein-

silver nanoparticle interactions to colloidal stability in acidic environments, Langmuir. 30 (2014) 12755–12764. https://doi.org/10.1021/la5033465.

[47] G. Wang, Y. Lu, H. Hou, Y. Liu, Probing the binding behavior and kinetics of silver nanoparticles with bovine serum albumin, RSC Adv. 7 (2017) 9393–9401. https://doi.org/10.1039/c6ra26089f.

[48] V. Banerjee, K.P. Das, Interaction of silver nanoparticles with proteins: A characteristic protein concentration dependent profile of SPR signal, Colloids Surfaces B Biointerfaces. 111 (2013) 71–79. https://doi.org/10.1016/j.colsurfb.2013.04.052.

[49] F. Cañaveras, R. Madueño, J.M. Sevilla, M. Blázquez, T. Pineda, Role of the functionalization of the gold nanoparticle surface on the formation of bioconjugates with human serum albumin, J. Phys. Chem. C. 116 (2012) 10430–10437. https://doi.org/10.1021/jp3021497.

[50] G. Gaucher, K. Asahina, J. Wang, J.-C. Leroux, Effect of Poly(N-vinyl-pyrrolidone)-block-poly(d,l-lactide) as Coating Agent on the Opsonization, Phagocytosis, and Pharmacokinetics of Biodegradable Nanoparticles, Biomacromolecules. 10 (2009) 408–416. https://doi.org/10.1021/bm801178f.